Application of tomographic techniques to the spatial-response mapping of antenna-coupled detectors in the visible

José María Rico-García, Luis Miguel Sanchez-Brea, Javier Alda

Applied Optics Complutense Group. Complutense University of Madrid. School of Optics. Av. Arcos de Jalon s/n. 28037 Madrid

A tomographic-like method based on the inverse Radon transform is used to retrieve the irradiance map of a focused laser beam. The results obtained from multiple knife edge measurements have been processed through a Kriging technique. This technique allows to map both the beam irradiance and the uncertainty associated with the measurement method. The results are compared with those achieved in the fitting of two orthogonal knife-edge profiles to a modeled beam. The application of the tomographic-like technique does not require any beam model and produces a higher SNR than the conventional method. As a consequence, the quality of the estimation of the spatial response map of an antenna-coupled detector in the visible is improved.

OCIS codes: 040.0040,130.0250

1. Introduction

Antenna-coupled detectors have deserved increased attention because of their unique characteristics for detecting and imaging in the infrared and millimeter bands [1, 2]. Down-scaled passive versions for the visible, named optical antennas [3–5], are being a subject of intense research. Plasmonics, biodetection technologies and near field optical microscopy are favored by the systematic study of these nanostructures [5, 6]. Then, it is a pertinent question to ask about the ability of antenna-coupled detectors

to detect light at visible wavelengths in the same fashion as IR antennas do. Some previous analysis exhibit response for IR antennas working in the visible part of the spectrum [7]. Nevertheless, an exhaustive examination of the detector behaviour should pay attention to the antenna spatial response, as one of the main merit figures of the device. As it has been pointed out in a previous work [8], the measurement of the spatial response would be greatly improved if the uncertainty of the irradiance map of the probe beam impinging on the detector were reduced as much as possible.

The aim of this paper is to describe a suitable measurement technique to map the irradiance $I(x, y)$ of the beam while decreasing the total uncertainty in the spatial response estimation. The technique is based on a tomographic-like method [9]. On the other hand, the measurement of $I(x, y)$ can be strongly affected by noise, thus decreasing the accuracy of the final result. In addition, it would be convenient to assess the uncertainty of the experimental data. We suggest a powerful statistical tool, known as Kriging [10], to deal with those aspects of the beam characterization.

The paper has been organized as follows. Section 2 explains the experimental set-up we have made use of. Section 3 is devoted to the estimation of $I(x, y)$ by means of the Radon transform method. We also compare these results with those obtained from the conventional Knife-edge technique [11] and estimate the uncertainty in retrieving the beam through the Radon transform by a statistical technique known as kriging. Section 4 describes the subsequent spatial response of an antenna-coupled detector

and, finally, the major conclusions of this paper are summarized in section 5.

2. Experimental set-up

The experimental set-up is shown in Figure 1. A laser diode emits a monochromatic beam at $\lambda = 658$ nm. The current driving the laser is electronically modulated following a square wave signal to work below and above its threshold current, $I_{\text{threshold}} = 45$ mA. As a result, the source current of the laser, I, can take the following values: $I_{\text{low}} = 20$ mA, and $I_{\text{high}} = 60$ mA. The laser is pigtailed to a monomode optical fiber. The output of the fiber is collimated by an aspheric lens, L_1. The collimated beam is partially transmitted by a (30/70) pellicle beam splitter at 45°. 70% of the light crosses through the $\frac{\lambda}{2}$ and $\frac{\lambda}{4}$ wave plates that are used for controlling the polarization state of the light. Finally, the radiation is focused by lens L_2 on the plane where the detector is placed. L_2 is another aspheric lens working in the visible $(600 - 1050$ nm) for an object at infinity, with an $N.A = 0.5$ and a focal distance $f' = 8$ mm. The response of the antenna-coupled detector is polarization-dependent. [7, 11]. In this case, the beam is linearly polarized at $\varphi = 68°$ taking as a reference the orientation of the antenna arms. The polarization azimuth is selected to align the $\vec{E}$ field along one of the signal–extraction bond pads. The photocurrent created by the antenna is converted to a voltage and preamplified. Then, it is directed to a lock-in amplifier synchronized with the modulation signal of the laser source.

The whole detection process is managed by a computer that is also in charge of the recording of the data.

The movement and positioning is controlled through the combination of a three-axis piezoelectric stages and a XY stepper motor. Thus, we have two kind of movements in the measurement process: a "coarse" movement, ruled by the XY stteper motor, whose nominal repeteability is ± 200 nm and a "fine" movement, in charge of the $3D$ stage, whose nominal repeteability is ± 5 nm.

The devices used here are Ni–NiO–Ni diodes coupled to integrated dipoles antennas [7] (see the inset of Figure 1). The dipole antenna has a total length of 6.7 μm and it was designed to get an optimum response at 10 μm. Its minimum feature size is about 200 nm. More details about them can be found in ref. [7].

Two different measurements are required to find the device spatial response. Firstly, it is essential to achieve a high quality estimation of the beam spot at the focalization plane. Once the beam waist plane is located and the device properly positioned on it, the second measurement is a two dimensional scan of the response of the device as a function of the location on the transversal plane previously selected. This measurement can be modeled as the convolution of the actual spatial response of the device with the irradiance map of the beam. Therefore, the map of the spatial response can be obtained as the deconvolution of the scan of the response of the device with the map of irradiance of the illuminating beam. This method has been successfully applied

to the spatial response characterization of a variety of antenna-coupled detectors and different beam distribution. [7, 11, 12] As we mentioned above, the scan is performed after placing the device at the point of maximum response, where the waist of the beam is located. This is a delicate operation since the antenna dimensions and the depth of focus of L_2 are tight restrictions to the detector placement. The first step to rightly place the device employs the illuminating source and a CCD camera (see Figure 1), which images the zone where the antenna is going to be placed. The antenna is moved until the camera achieves a well-defined image of the antenna structure and bondpads. This placement is can be considered a first order approximation to a more precise positioning of the device. Then, the fine positioning is done by maximizing the response of the detector. Once this process is finished, we assume that the beam waist location coincides with the antenna.

3. Beam measurement

It has been shown that the weakest link in the measurement of the spatial response of antenna-coupled detectors, no matter the wavelength of the source, is the beam characterization [8]. Generally, the beam must be determined in a grid of n^2 points, where the scan is done. When the conventional knife-edge method is used, only $2n$ points are measured. The variation of $I(x, y)$ in the grid is found through a fitting of the measured data - the profiles $P_{0^\circ}(x)$ and $P_{90^\circ}(y)$ at $\theta = 0^\circ$ and $\theta = 90^\circ$ - to a beam

model [11]. As a result, the uncertainty in the spatial response is strongly affected by the lack of information that this method entails. As this is the most significant source of error in the whole process of measurement [8], it would be convenient to get information of the beam not only at 0° and 90° but also at different angles, thus covering as much as possible the region where the spot may change. The Radon transform method provides a better knowledge of the beam irradiance map [9,13–15], since the reconstruction of the latter takes advantage of the information kept in other different profiles than $P_{0^\circ}(x)$ and $P_{90^\circ}(y)$. Consequently, we expect a far more higher fidelity in the beam reconstruction when this procedure is used.

In the following, we will compare the results obtained from a tomographic-like method that uses a large number of knife edge measurements, with the results obtained from the application of the conventional two knife-edge method. Some details of the set-up can be seen in the inset of Figure 2. The knife-edge is placed on the plane showing the largest irradiance (beam waist plane). A large area photodetector under the blade records the non-blocked signal. The amplitude of the latter depends on the knife-edge position, u. The blade moves along the u axis with the aid of the three-axis stage locked at the beam waist plane (around $z = f'$). All the recorded signals are shown in Figure 2. The variables $\{u, v\}$ are related to $\{x, y\}$ by means of a rotation of angle θ.

3.A. Measurement of the beam by using the Radon transform

The set of profiles taken at different angles - also called sinogram - is related to the beam irradiance map through its direct Radon transform [9, 14, 15] and defined as

$$P(u,\theta) = \int_{-\infty}^{\infty}\int_{-\infty}^{\infty} I(x,y)\delta(u - x\cos\theta - y\sin\theta)dxdy, \tag{1}$$

where θ is the angle of rotation and u is a variable accounting for the knife-edge location. Therefore, $P(u,\theta)$ can be considered as a line integral of the intensity map $I(x,y)$ along the straight line $u = x\cos\theta + y\sin\theta$. We intend to recover $I(x,y)$ through a new set of profiles, $Q(u',\theta)$. They represent the amount of accumulated power measured by the photodetector at different angles and, as Quabis *et al.* [9] have pointed out,

$$Q(u',\theta) = \int_{u'}^{\infty} P(u,\theta)du, \tag{2}$$

so

$$P(u',\theta) = -\frac{\partial Q(u',\theta)}{\partial u'}. \tag{3}$$

Therefore, the Radon transform of the beam at focus is proportional to the partial derivative of $Q(u',\theta)$. The inverse Radon transform can be computed [13] using the following equation

$$I(x,y) = \mathcal{R}^{-1}(P(u,\theta)) = \int_0^{\pi}\int_{-\infty}^{\infty} d\rho d\theta|\rho|[\int_{\infty}^{\infty} P(u,\theta)e^{-i\rho u}du]e^{i\rho(x\cos\theta + y\sin\theta)},, \tag{4}$$

based on the so-called Fourier-slice theorem [13]. When implemented in a computer, it is known as the "Filtered back-projection algorithm" [9, 13].

In order to perform the Radon transform, we have measured 18 accumulated profiles every $\Delta\theta = 10^\circ \pm 2^\circ$. A successful inversion of $P(u,\theta)$ requires normalizing, centering and interpolating the whole set of measured profiles in the variable u'. Figure 2 shows $Q(u',\theta)$ after completing these tasks. The next step is to compute the derivative of $Q(u',\theta)$. At this stage, the kriging filter, that will be explained in subsection 3.C, is applied to the output of $\partial_{u'}Q(u',\theta)\ |_u$. Not only an average sinogram, $\hat{P}(u,\theta)$, is obtained, but also an estimation of the error in the former, $\Delta\hat{P}(u,\theta)$. Both are computed numerically when solving the kriging equations. Each slice of $\hat{P}(u,\theta)$ at $\theta = \theta_0$ represents an integrated profile in such direction. All the slices are used in order to retrieve the irradiance map accurately. The sinogram is plotted in figure 3. Figure 4 shows the retrieved map of the beam after inverting $\hat{P}(u,\theta)$. Despite the fact of being close to a Gaussian beam, there are clear deviations from this ideal behaviour.

If we took fewer number of profiles, the angular sampling would be worse and the reconstruction of the irradiance map would not be as faithful as it would be with an increased number of profiles. As a matter of fact, by choosing 18 profiles we look for a balance between measurement time and accuracy in the retrieving process. However, an optimum number of profiles should exist. Taking less or more profiles than this optimum number should produce undersampled or oversampled maps. Unfortunately, this optimum number is beam-dependent and it can only be known "a posteriori".

After analyzing the results from our 18 profiles we could conclude that the beam shape retrieved by the inverse Radon transformation begins to be stable after taking, at least, 9 profiles.

The Radon transform method is helpful not only for its high SNR figure, as it will be demonstrated in the next section, but also because of its ability to reconstruct $I(x, y)$ as close to the real beam as the measurement conditions allow.

In spite of the aforementioned advantages, the inversion of $\hat{P}(u, \theta)$ is still not fully reliable. The zero frequency component of the spatial spectrum of $I(x, y)$ is lost in the inversion process [13]. Fortunately, this fact is not as troublesome as it could seem. The zero frequency component is equal to the total power falling onto the detector, $W = \int_{-\infty}^{\infty} \int_{-\infty}^{\infty} I(x, y) dxdy$, which can be easily measured, not to mention that a normalized beam is enough to compute the normalized spatial response of the detector.

3.B. Measurement of the beam by using two orthogonal knife-edge

For the sake of comparison with the method previously used to obtain the map of irradiance, we have used the knife-edge data to fit selected orthogonal pairs of knife-edge measurements with those derived from an appropriate model of the beam. This model contains diffractive effects and the most probable aberrations of the experimental set-up [11]. The irradiance map is expressed analitically as the convolution

of a Gaussian beam with the Airy comatic spot, because we expect to find a residual coma contribution due to possible misalignements in the optical elements of the experimental arrangement [8, 11, 16, 17].

$$E(x,y) = e^{-(\frac{x^2+y^2}{\omega_0})} * \left\{ \frac{2J_1(\nu)}{\nu} - \Big(\cos\phi \frac{2J_4(\nu)}{\nu}\Big)\alpha \right.$$
$$\left. -\frac{1}{2\nu}\Big(\frac{J_1(\nu)}{4} - \frac{J_3(\nu)}{20} + \frac{J_5(\nu)}{4} - \frac{9J_7(\nu)}{20} - \cos 2\phi(\frac{2J_3(\nu)}{5} + \frac{3J_7(\nu)}{5})\Big)\alpha^2 \right\}. \quad (5)$$

Here, $*$ means convolution; ω_0 is the beam waist at focus; α is the amount of coma in wavelength units;ϕ is the orientation of the comatic spot; $\nu = 2\pi a\sqrt{x^2+y^2}/\lambda f'$, where $a = 4$ mm is the radius of the aperture, λ is the wavelength and f' is the focal distance of the focusing lens; J_k are the Bessel functions of k order and, finally, ω_0, α and ϕ are the fitting parameters. This model has been fitted with the 9 orthogonal pairs of knife-edge measurement that can be extracted from the 18 knife-edge curves used in the tomographic method. In our case, we get as optimum values $\omega_0 = 4.6 \pm 0.3$ μm, $\phi = 50^\circ \pm 10^\circ$ and $\alpha = 0.7 \pm 0.3$. The uncertainties have been estimated from the 9 couples of orthogonal profiles (after applying the kriging filter to $\partial_{u'}Q(u',\theta)$), except for ϕ, whose error is the resolution of the rotator.

The map of the beam and its error is shown in Fig. 5. There is a noticeable difference between the beam shape retrieved by the 2 knife-edges and fitting method, and the beam shape recovered by means of the Radon transform method. The use of two orthogonal profiles and a beam model does not take into account the fine angular

variations of the irradiance map in the beam tails. Therefore, the Radon transform is better suited to retrieve the irradiance map than the two-profile knife-edge method.

3.C. Kriging filtering and error estimation

The inversion of $P(u,\theta)$ involves a serious problem, i.e, the derivative operator $\partial_{u'} \xrightarrow{\mathcal{F}} ik'$ ($\mathcal{F}$ is the Fourier transform) plays the role of a high-pass filter. In fact, it enhances the importance of the high-frequency components held in $Q(u',\theta)$ whose effect is noticeable in $P(u,\theta)$. Unfortunately, these high-frequency components are typically associated with noise and, in consequence, they reduce the fidelity in the beam reconstruction. Some ideas have been applied to filter those undesirable components out from $P(u,\theta)$. For instance, a remarkably effective technique is the Savitzky-Golay algorithm [9, 14, 15]. Nonetheless, as far as we know no estimation of the error in inverting $P(u,\theta)$ is done. In this article, we suggest the use of the Kriging methodd to solve these difficulties by relying on a statistical-based filtering approach. [10].

Kriging is a family of linear algorithms to estimate both spatial-dependent magnitudes and their variance. The fitting is optimum in the least-square sense, when only a noisy, limited number of data are available [10]. Kriging has been succesfully applied in optics for the analysis of diffraction minima in far field diffractometry and in image processing [18–21]. Kriging methods take advantage of the spatial correlations of the signal under study. Moreover, the Kriging equations can be given as a convolution

product if the magnitude is regularly sampled, making easier both the filtering post-processing and the estimation of the variance of the magnitude thus analyzed [20,21]. An illustrative example can be seen in Figure 6, where the effect of a Golay filter of order 5 and 45 points [14] is compared with the effect of the Kriging filter on the same profile obtained at $\theta = 70^\circ$ (this profile has been arbitrarily chosen).

Paying attention to the sinogram error represented in Fig. 3, we may conclude that it is practically independent from θ. This means that all the slices in $\Delta\hat{P}(u,\theta)$ are equivalent, and all the information contained in the sinogram error can be comprised in any of its slices. On the other hand, the farther the point (u,θ_0) is from the center of a profile at a given angle θ_0, the higher the error is at this point. As a consequence, the quality of the measurements in the beam tails is worse than those measurements made in the center of the spot

The knowledge of $\Delta\hat{P}(u,\theta)$ paves the way to define two error curves for each knife-edge profile,

$$P^{\pm}_{error} = \hat{P} \pm \Delta\hat{P}. \tag{6}$$

An advantage of applying a kriging filter to the derivative of $Q(u',\theta)$ is its capability to estimate the error, $\Delta I(x,y)$, of the irradiance map. This error is defined in terms of the error obtained for the sinogram. Firstly, new error curves for $I(x,y)$ can be

defined as,

$$I^{\pm}_{error} = \mathcal{R}^{-1}(P^{\pm}_{error}). \tag{7}$$

Consequently, the error ΔI is

$$\Delta I = \mathcal{R}^{-1}(\Delta \hat{P}) = \frac{I^{+}_{error} - I^{-}_{error}}{2}. \tag{8}$$

Finally, a straightforward computation of the Signal-to-Noise Ratio (SNR) follows from this equation

$$\text{SNR} = \frac{I(x,y)}{\Delta I(x,y)}. \tag{9}$$

Figure 4 shows the results for SNR. As we predicted before, the closer the point (x, y) is to the center of the beam, the lower the fluctuations are over the average value of $I(x, y)$. The maximum SNR is $SNR_{max} = 29.36$. When the beam is retrieved using the Golay filter, the smooth variations of the spot are lost as Fig. 7 reveals.

Figure 5 shows the beam and its SNR estimated through the method based on a beam model, proving that the SNR is worse than the Radon transform SNR (the maximum value is, in this case, $SNR_{max} = 10.15$). Furthermore, the shape of the former differs from the shape of the beam reconstructed through the Radon transform method. The approach presented in this work is expected to provide a closer estimation of the real beam than those based on a fitting procedure, because of the larger amount of information that it can process. Therefore, the representation of the beam spot is dramatically improved when the Radon transform method with and

adecuate noise filtering is adopted.

To sum up: the Radon transform method provides a more accurate estimation of the beam irradiance map than the fitting procedure, on the grounds that it considers the variation of the integrated profiles in the whole angular range $\theta = [0, 2\pi)$. The application of the kriging method has made possible to reduce noise and also to include a map of the uncertainty of the beam irradiance distribution. On the other hand, no more modeling and further assumptions about the presence of a given aberration are needed.

4. Deconvolution of the antenna response

The irradiance map is needed when recovering the spatial response of the device, and, as it will be demonstrated, its influence in the latter can be crucially important. The response of an antenna-coupled detector under the probe beam is [11]:

$$S(x, y) = \int_{-\infty}^{\infty} \int_{-\infty}^{\infty} I(x', y') R(x - x', y - y') dx' dy', \tag{10}$$

where $R(x, y)$ is the spatial response of the device and $S(x, y)$ represents the scan map. $R(x, y)$ can be reconstructed from the knowledge of $I(x, y)$ and $S(x, y)$ if a deconvolution algorithm is applied on (10). We have choosen the Richardson-Lucy algorithm, which has been successfully employed in deconvolving the spatial response of antenna-coupled detectors [8, 11] both in the infrared and in the visible. $S(x, y)$ is measured on a grid with $\Delta_x = \Delta_y = 0.150$ μm, taking a window of 15×15 μm^2.

Then, the spatial response is retrieved from an iterative process of deconvolution - $I(x, y)$ must be determined beforehand -.

Figure 8 displays the spatial maps computed with the two methods: the tomographic method and the conventional orthogonal knife-edge pair. Both share some common features, like the maximum central peak at the position of the antenna or the two lateral, minor peaks linked to the metallic connectors of the structure [7]. However, there are noticeable differences between them. For instance, the distance between the maximum peak and the lateral lobes are not the same for each map. Furthermore, the centroid of the map computed from the beam model seems to be displaced from the position of the centroid of the map computed from the Radon transform method. This is due to the model that it has been adopted to fit the data. Such a fact sheds light on the way the Radon transform improves the measurement of the spatial response of the detector. If we had selected another model, the spatial map would have not be the same. In other words, our lack of knowledge about the beam makes more difficult to get a reliable measurement of the spatial map, because we need to guess the analytical form of the beam prior to any fitting. This problem would be circumvented if the method could handle moreinformation about the beam, as the Radon transform method actually does.

5. Conclusions

In this paper we have demonstrated how a tomographic-like technique can be applied to the improvement in the characterization of the spatial response of an antenna-coupled detector. Due to the experimental conditions involved in this contribution, the probe beam is expected to be weakly aberrated and weakly diffracted. The almost-Gaussian beam profile has been properly retrieved by the proposed method. This improvement is possible because the beam SNR is larger than the one obtained from the use of two orthogonal knife-edge profiles and its fitting to a model. For the same beam and measurement data, the SNR of the beam irradiance jumps from 10.15 to 29.36 when moving to the method proposed in this paper. As far as it has been proved [8] that the main source of uncertainty of the spatial response map is coming from the beam irradiance estimation, we may infer that the spatial response is of better quality.

One of the key elements of the method is the use of Kriging techniques for the processing of the experimental data. In our case, the kriging technique filters the high frequency components out of the derivative of the knife-edge data to obtain the sinogram. This is critical for the inverse Radon transform to produce a smooth irradiance map. On the other hand, kriging provides by itself the uncertainties associated to the processed data. These uncertainties are finally represented as a map allowing a

graphical representation of the SNR of the irradiance distribution. The SNR is much better at the maximum of the beam irradiance and decreases towards the tail of the beam distribution.

We conclude that the proposed method for estimating the beam irradiance map is better than the one previously reported because it does not need any kind of modeling. On the other hand, the number of available data points is greater than the conventional method using two orthogonal knife-edges. This fact, along with the use of the kriging method, makes the spatial map measurement more reliable and more accurate.

6. Acknowledgments

This work has been partially supported by the project TEC2005-1882 from the Ministerio de Educacion of Spain. The devices tested in these experiments have been supplied by the Infrared Systems Lab of the College of Optics and Photonics (CREOL) of the University of Central Florida, headed by Prof. Glenn Boreman. L.M. Sanchez-Brea is currently contracted by the Universidad Complutense de Madrid under the "Ramón y Cajal" research program of the Ministerio de Educación y Ciencia of Spain. J. M. Rico -García acknowledges a grant from the Universdad Complutense of Madrid.

References

1. M. Abdel Rahman, B. Monacelli, A. Weeks, G. Zummo and G. D. Boreman,"Design, fabrication and characterization of antenna-coupled metal-oxide-metal diodes for dual-band detection". Opt.Eng, **44**, 066401, (2005).

2. F. J. González, B. Ilic, J. Alda, and G.D. Boreman, "Antenna-coupled infrared detectors for imaging applications", IEEE J. Sel. Topics Quantum Electron, **11**, 117-120, (2005).

3. P. Mühlschlegel, H.-J. Eisler, O. J. F. Martin, B. Hecht, D. W. Pohl,"Resonant optical antennas", Science, **308**, 1607-1609, (2005)

4. K. B. Crozier, A. Sundaramurthy, G. S. Kino, C. F. Quate,"Optical antennas: Resonators for local field enhancement" J. Appl. Phys., **94**, 4632-4642, (2003)

5. T. H. Taminiau, R. J. Moerland, F. B. Segerink, L. Kuipers, N. F. van Hulst, "$\lambda/4$ resonance of an optical monopole antenna probed by single molecule fluorescence", Nano Lett., **7**, 28-33 (2007)

6. P. Bharadwaj, P. Anger, and L. Novotny "Nanoplasmonic enhancement of single molecule fluorescence" Nanotech., **18**, 044017. (2007)

7. C.Fumeaux, J.Alda, G.Boreman, "Lithographic antennas at visible frequencies", Opt. Lett. **24**, 1629-1631,(1999).

8. J.M. López-Alonso, B.Monacelli, J.Alda, G.Boreman, "Uncertainty analysis in

the measurement of the spatial responsivity of infrared antennas", Appl. Opt. **21**, 4557–4568 (2005)

9. S. Quabis, R. Dorn, M. Eberler, O. Glöckl, G. Leuchs, "The focus of light – theoretical calculation and experimental tomographic reconstruction", Appl. Phys. B **72**, 109–113 (2001)
10. N. Cressie, *Statistics for Spatial Data* (Wiley, New York, 1991).
11. J.Alda, C.Fumeaux, I.Codreanu, J. Schaefer, G.Boreman, "A deconvolution method for two-dimensional spatial-response mapping of lithographic infrared antennas", Appl. Opt. **38**, 3993–4000 (1999)
12. F. J. González, G. Boreman, "Comparison of dipole, bowtie, spiral and log-periodic IR antennas", Inf. Phys. & Technol. **46**, 418-428, (2005)
13. P.Toft, "The Radon transform – Theory and implementation", Ph.D Thesis, Department of Mathematical Modelling, Technical University of Denmark, (1996), http://petertoft.dk/PhD
14. R. Dorn, S. Quabis and G. Leuchs "The focus of light – linear polarization breaks the rotational symmetry of the focal spot", J. Mod. Opt. **50**, 1917–1926 (2003)
15. R. Dorn, S. Quabis and G. Leuchs, "Sharper Focus for a Radially Polarized Light Beam", Phys. Rev. Lett. **91**, 233901-1–233901-4, (2003).
16. O.Mendoza-Yero,J.Alda "Irradiance map of an apertured Gaussian beam affected

by coma", Opt. Commun. **271**, 517-523, (2007).

17. M. Born and E. Wolf, *Principles of Optics*, (Pergamon Press, Oxford, 1989).

18. E. Bernabeu, I. Serroukh, L.M. Sanchez-Brea "A geometrical model for wire optical diffraction selected by experimental statistical analysis" Opt. Eng., **38**, 1319-1325 (1999)

19. W.Y.V. Leung, P.J. Bones, R.G. Lane,"Statistical interpolation of sampled image" Opt. Eng., **40**,547-553 (2001)

20. L.M. Sanchez-Brea and E. Bernabeu,"Determination of the optimum sampling frequency of noisy images by spatial statistic", Appl. Opt. **44**, 3276-3283 (2005)

21. L.M.Sanchez-Brea, E. Bernabeu "Uncertainty estimation by convolution using spatial statistics", IEEE Trans. Image Process. **15**, 3131-3137, (2006).

7. Figures and captions

1. Fig.1 Experimental set-up

2. Fig.2 Profiles $Q(u', \theta)$. The spatial step is $\Delta x = 35.3$ nm. 18 profiles have been measured from 0° to 170° each $\Delta\theta = 10° \pm 2°$. The inset contains a diagram of the measurement of $Q(u', \theta)$

3. Fig.3 Sinogram $\hat{P}(u, \theta)$ and sinogram error $\Delta\hat{P}(u, \theta)$. The sinogram error is practically independent from θ, meaning that all the information about the

error in the measurement of $\hat{P}(u,\theta)$ is contained in any of the slices of $\Delta\hat{P}(u,\theta)$. However, a complete reconstruction of the beam needs all the slices.

4. Fig.4 Beam irradiance map in arbitrary units employing the Radon transform and its SNR

5. Fig.5 Beam irradiance map in arbitray units employing the fitting method and its SNR

6. Fig.6 Kriging *vs* Golay filtering approaches. The figure shows the derivative of $Q(u',\theta = 70^{\circ})$ and the Golay filter and the Kriging filter estimations on it. In the inset, it has been added the Kriging error curves.

7. Fig.7 Beam irradiance map in abitrary units after applying the Golay filter. Please note that the negative values of the irradiance map are unphysical. They are artifacts inherently linked to the noise induced by the derivative of $Q(u',\theta)$ in the beam tails, where the irradiance is close to zero

8. Fig.8 Top: A, the spatial response computed with the Radon transform method. Bottom: B, the spatial response get from the fitting to a beam model

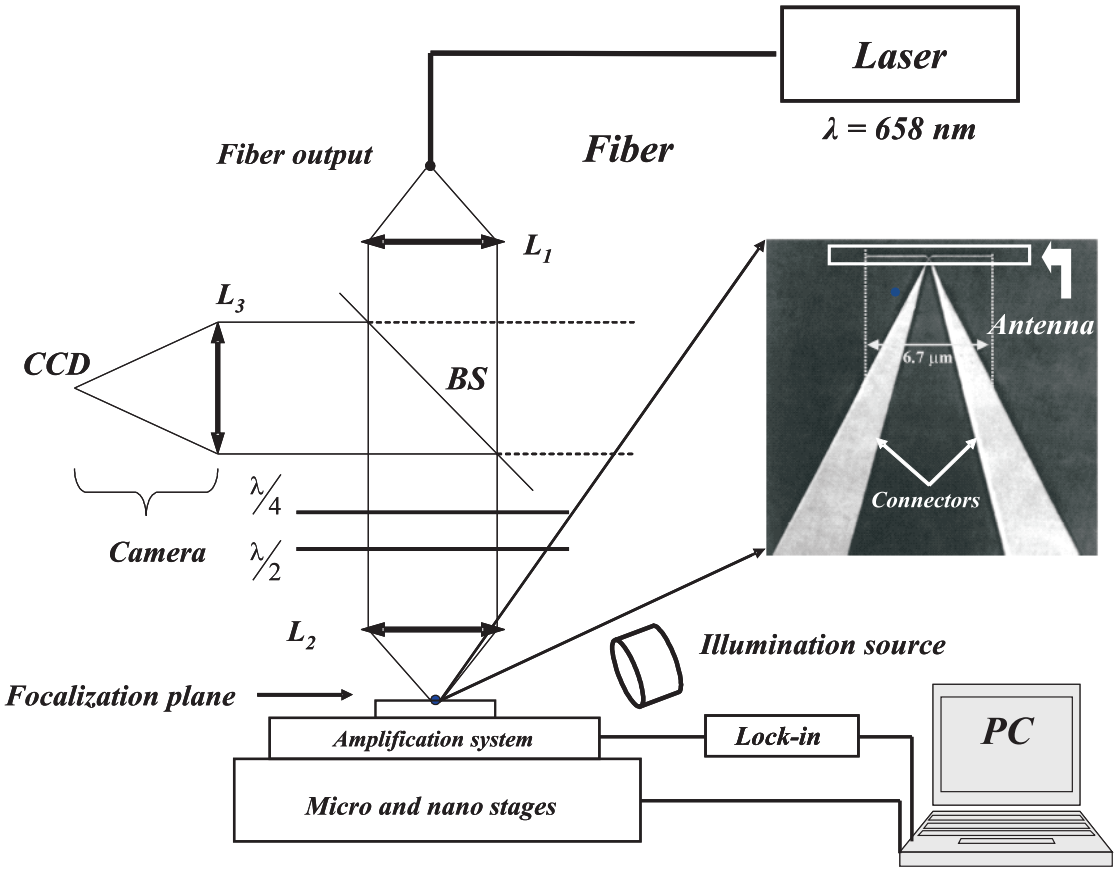
Laser
λ = 658 nm
Fiber output
Fiber
L1
L3
CCD
BS
λ/4
Camera
λ/2
L2
Focalization plane
Antenna
6.7 μm
Connectors
Illumination source
Amplification system
Lock-in
PC
Micro and nano stages

Fig. 1.

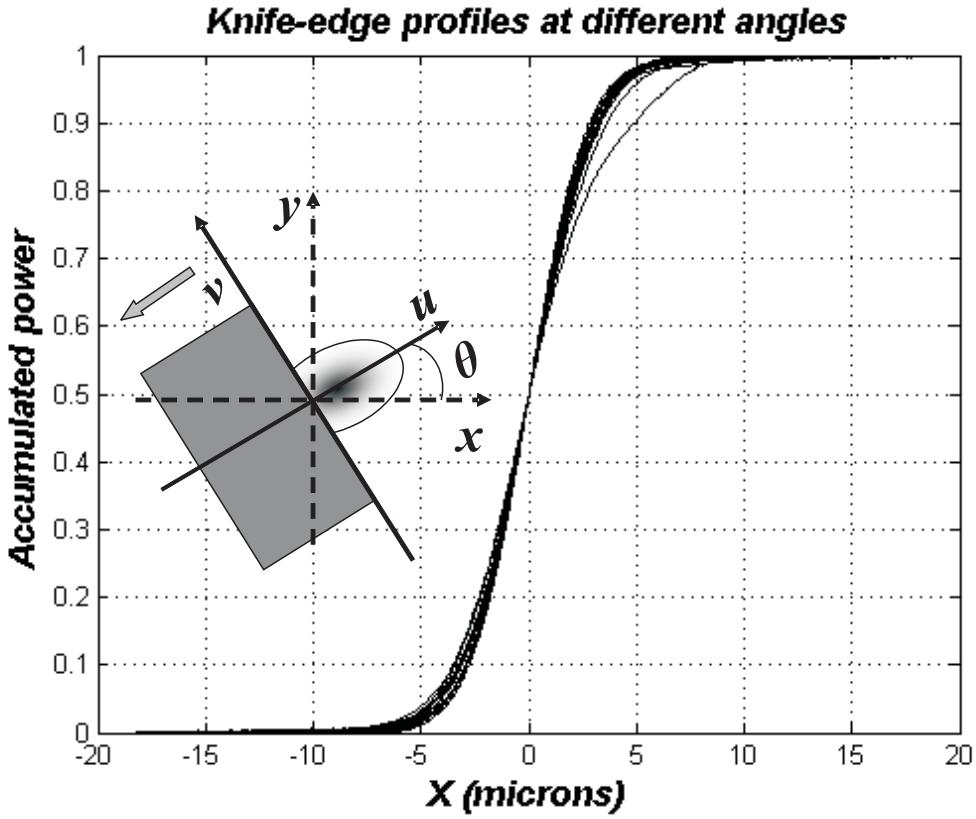
Knife-edge profiles at different angles
Accumulated power
X (microns)
y
v
u
θ
x
1
0.9
0.8
0.7
0.6
0.5
0.4
0.3
0.2
0.1
0
-20
-15
-10
-5
0
5
10
15
20

Fig. 2.

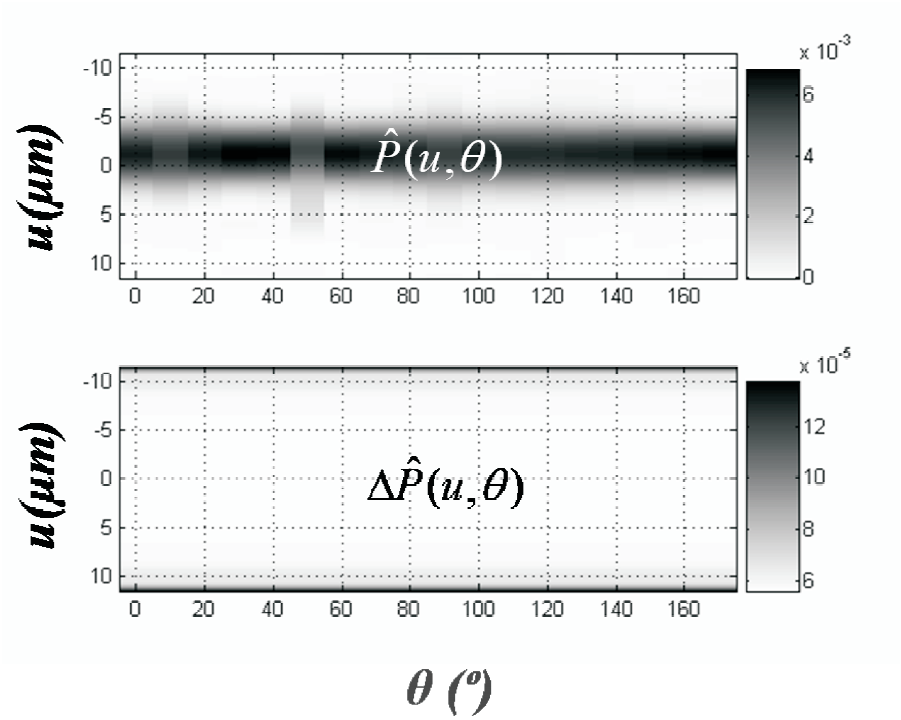

Fig. 3.

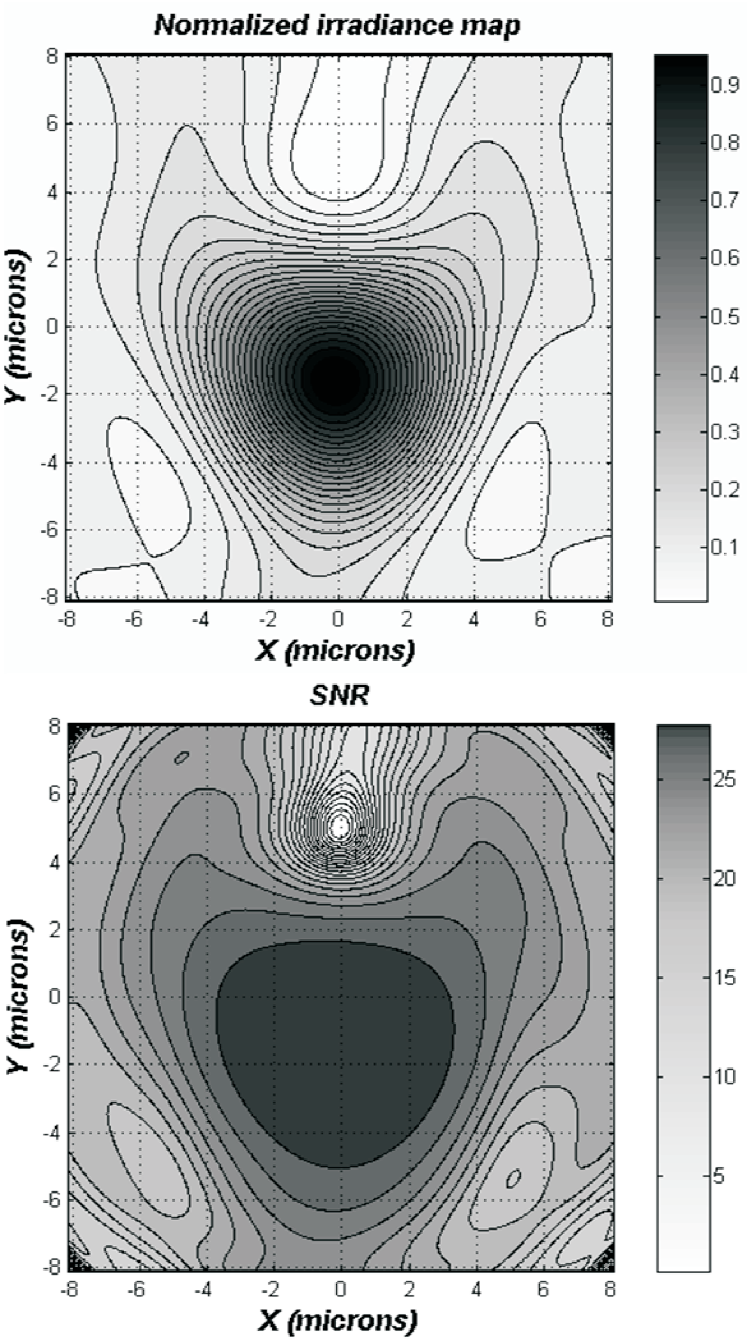
Normalized irradiance map
Y (microns)
X (microns)
SNR
Y (microns)
X (microns)

Fig. 4.

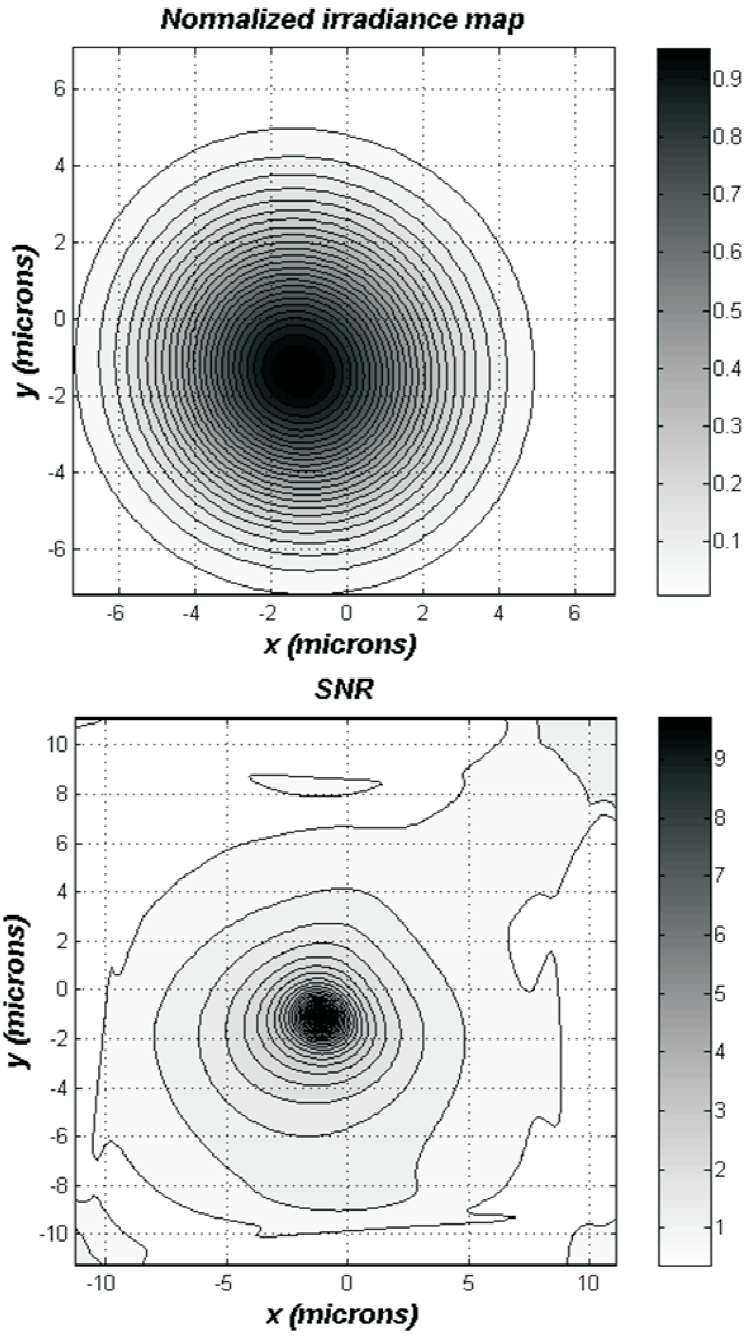
Normalized irradiance map
y (microns)
x (microns)
SNR
y (microns)
x (microns)

Fig. 5.

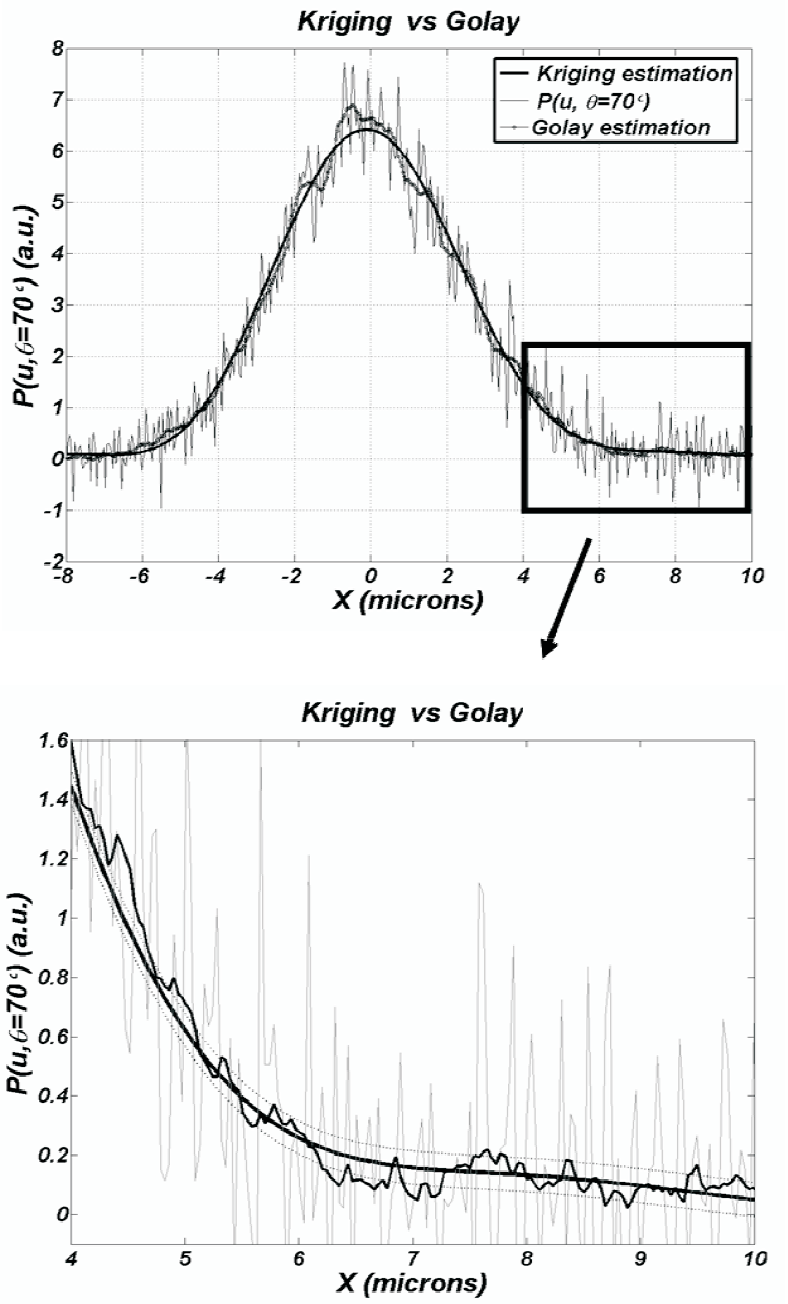
Kriging vs Golay
Kriging estimation
P(u, θ=70°)
Golay estimation
P(u,θ=70°) (a.u.)
X (microns)
Kriging vs Golay
P(u,θ=70°) (a.u.)
X (microns)

Fig. 6.

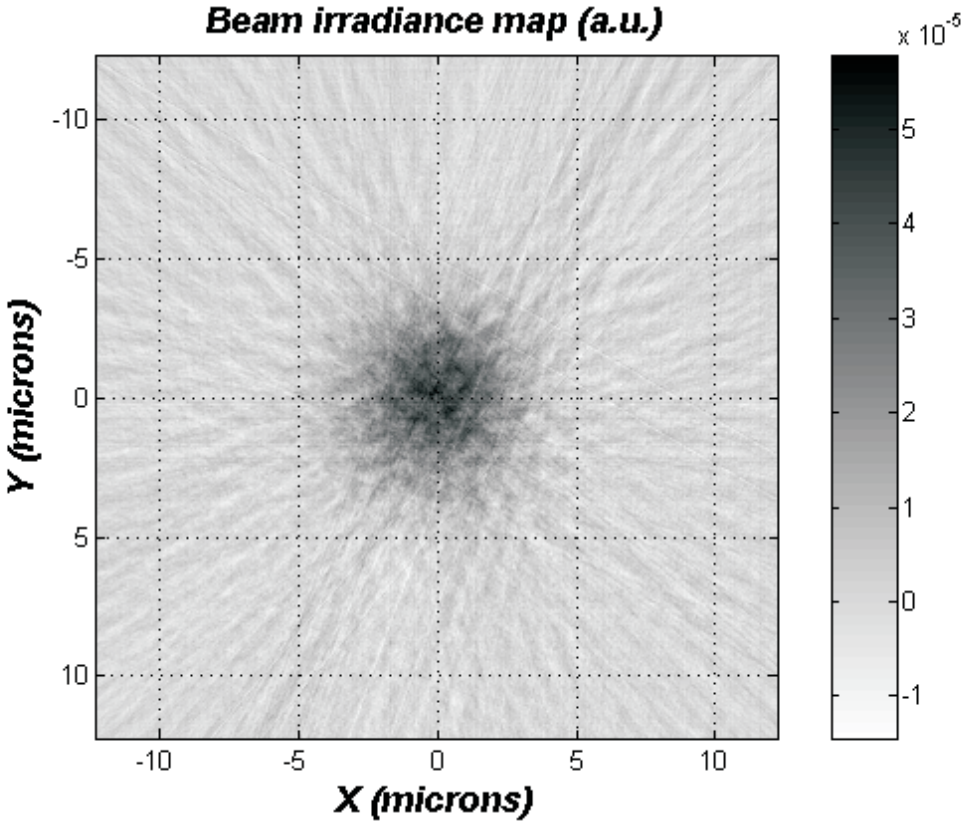
Beam irradiance map (a.u.)
x 10^-6
5
4
3
2
1
0
-1
-10
-5
0
5
10
Y (microns)
-10
-5
0
5
10
X (microns)

Fig. 7.

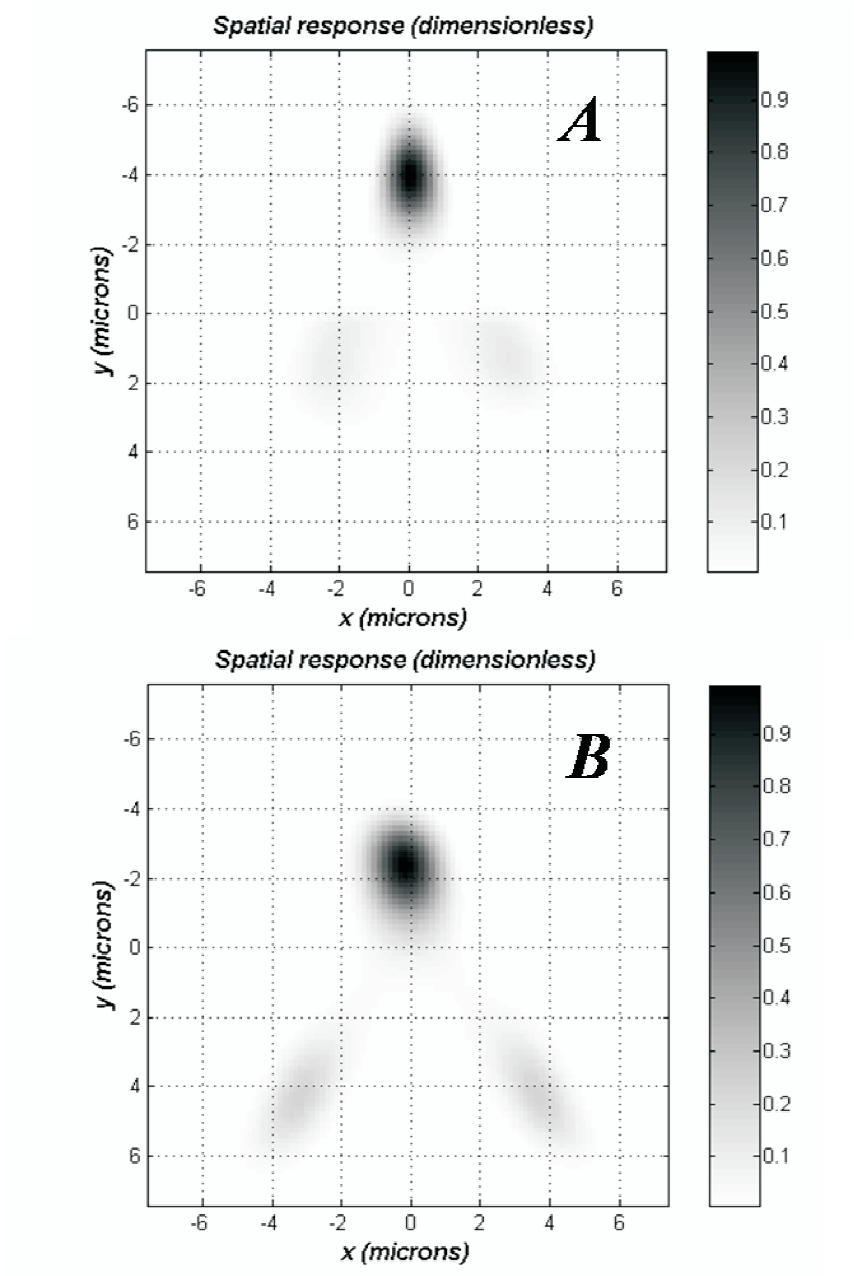
Spatial response (dimensionless)
A
y (microns)
x (microns)
Spatial response (dimensionless)
B
y (microns)
x (microns)

Fig. 8.